Pol. J. Environ. Stud. Vol. 34, No. 3 (2025), 3033-3045
DOI: *10.15244/pjoes/188283* ONLINE PUBLICATION DATE: 2024-09-24

Original Research

Transforming *Conocarpus* Hedge Waste into a Highly Effective Iron/Manganese Nanocomposite Biochar for Efficient Methylene Blue Dye Removal from Aqueous Solution

Abdulrahman Ali Alazba[1, 2], Muhammad Shafiq[2]*, Muhammad Tahir Amin[3]

[1] Agricultural Engineering Department, King Saud University, P. O. Box 2460, Riyadh 11451, Kingdom of Saudi Arabia
[2] Alamoudi Water Research Chair, King Saud University, P. O. Box 2460, Riyadh 11451, Kingdom of Saudi Arabia
[3] Civil and Environmental Engineering Department, College of Engineering, King Faisal University, Al-Ahsa 31982, Kingdom of Saudi Arabia

Received: 10 March 2024
Accepted: 5 May 2024

Abstract

In this study, we delve into the synthesis of Conocarpus (pruning waste) biochar (C.biochar) and its composite with Iron/Manganese (Fe/Mn-C.biochar) through a modified wet impregnation method. Batch adsorption experiments were conducted to evaluate the methylene blue (MB) removal efficiency of C.biochar and Fe/Mn-C.biochar composite from aqueous solution. Several key factors were analyzed, namely, contact time, adsorbent dose, pH level, and MB concentration. Fe/Mn-C.biochar composite showcased remarkable MB removal efficiency, exhibiting a 100% removal rate, whereas C.biochar alone removed 25% MB. Adsorption capacity peaked at 97.41 mg g^{-1} within 60 minutes of contact time. pH values significantly influenced the adsorption process, indicating improved removal efficacy at both acidic and alkaline conditions. This improvement is potentially attributed to surface complexation and the interaction between metal ions in the composite. A kinetic study was conducted, favoring the pseudo-second-order model. MB dye removal data exhibited best fit to Temkin and D–R models that showcased chemisorption, reinforcing the suitability of the composite for successful adsorption. FTIR analysis revealed the presence of diverse functional groups in the synthesized nanocomposites. For Fe/Mn-C.biochar composites, the IR analysis exhibited peaks associated with metal-oxygen vibrations, emphasizing the incorporation of Fe and Mn. However, the peak intensities related to Fe and Mn reduced after the adsorption of MB, suggesting the creation of complexes between the dye molecules and metal oxides. Additionally, morphological studies and EDS analysis further confirmed that the weight ratio of Fe and Mn decreased in the MB-adsorbed nanocomposites. These mechanisms provide a sustainable and optimistic solution for the elimination of MB dye.

Keywords: Fe/Mn-C.biochar nanocomposite, Conocarpus waste, adsorption kinetics and isotherms, surface complexation, methylene blue dye, sustainable adsorbent

*e-mail: msrana@ksu.edu.sa
Tel: +966114673737; Fax: +966114673739

Introduction

The scarcity of water is a significant worldwide issue, placing immense pressure on both the environment and humanity [1]. Communities worldwide are facing a growing need for freshwater that frequently exceeds the available supply, presenting a significant challenge. For example, this shortage of water is more noticeable in arid areas where population densities are increasing, and water resource management strategies are inadequate [2]. As agricultural land becomes scarcer, risks to agriculture, industry, and overall social health also increase [3, 4]. The widespread issue of water pollution only adds to this challenge, creating a new layer of complexity in the global water crisis. Industrial chemicals, including methylene blue (MB), play an important role in the contamination of water sources. It is commonly used in industries like textile and printing because of its unique chemical properties that make it necessary to be removed from water systems [5]. The continuity of these pollutants within natural aquatic environments threatens species richness, ecosystem services, and health outcomes among people who depend on such sources [6].

Water pollution should be addressed because it is very critical in ensuring that there is sufficient clean water. This is because standard water treatment approaches usually fail to remove particular contaminants, such as MB, effectively [7]. As a result, the need for innovative and sustainable water purification technologies is increasing. This brings us to the focal point of our investigation: There is a need to investigate synergistic mechanisms of the biochar with Fe/Mn in MB adsorption. Currently, considerable research has been dedicated to biochar derived from diverse materials using the pyrolysis technique, which is regarded as a potential substance for water treatment [8], and at the same time, a mixture of iron (Fe) and manganese (Mn) coupled with biochar is a very interesting pathway for improved adsorption capacity [9].

A highly carbonaceous material, biochar, is obtained through the process of pyrolysis with biomass and has been attracting a lot of attention due to its diverse uses in water treatment [10]. Compared to many other adsorbents that are used for removing pollutants such as heavy metals and organic dyes, biochar has proven to be a very efficient one. Lu et al. discussed the high adsorption capabilities of biochar derived from agricultural wastes to remove organic contaminants in the water [11]. Nevertheless, despite these virtues, biochar possesses many limitations, such as the limited affinity for some pollutants, requiring additional improvements towards customization based on the water treatment application niches [12]. To deal with the limitations of current biochar, significant investments were made in developing modern composite materials. One of such emerging composites is the Fe/Mn-C.biochar composite. This composite shows a particular Fe, Mn, and C composition that strongly increases the adsorption capacity, especially for certain contaminants. Research has shown that the Fe and Mn biochar addition improves the selectivity levels as well as affinity towards target compounds, hence a substantial increase in the overall performance of water treatment is observed.

In a recent study that focused on improving the removal of contaminants, Shi et al. investigated both the metallic and biochar oxides effects in combination [13]. While these composite materials show an enhanced absorption capacity, weaknesses such as agglomeration and limited stability under some conditions are still inevitable disadvantages [14]. Balancing the adsorption efficiency and stability of materials is very important for the operation of biochar-metals composite systems.

Among the large number of combinations between metal and other metals that have been investigated, the Fe/Mn binary system has proven to be an excellent direction [15]. The catalytic activity and redox potential of Fe/Mn composite contribute significantly to enhancing the adsorption efficiency of biochar [16]. A recent study showed that Fe/Mn-loaded biochar has great potential for textile wastewater treatment [17]. Thus, addressing the limitations of biochar and metals for the synthesis of metal-loaded biochar offers an attractive and effective wastewater treatment. The study of these materials is caused by their characteristics to work synergistically together, thus forming a system that works more effectively and efficiently in eliminating MB from water.

Material and Methods

Materials

Ferric chloride hexahydrate ($FeCl_3 \cdot 6H_2O$) and manganese dichloride tetrahydrate ($MnCl_2 \cdot 4H_2O$) were purchased from Surechem Products Limited, UK. MB was purchased from Sigma-Aldrich, Co., Spruce Street, St. Louis. The chemicals utilized in this study were analytical grade. The aqueous solution was prepared using distilled water.

Material Synthesis

Biochar Synthesis

The waste from pruning Woody Conocarpus was gathered from the male campus of King Saud University in Riyadh, Saudi Arabia. The biomass was thoroughly washed multiple times using ultrapure water, after which it was oven-dried for 48 hours at 105°C, and finally ground. The resulting particles from grinding were stored for the next stage.

The pristine C.biochar was synthesized by subjecting the biomass (Woody Conocarpus pruning) to pyrolysis when heated to 800°C for three hours at a rate of 5°C per minute in a Nabertherm GmbH (Germany) box furnace with limited oxygen. The obtained biochar underwent several washes with ultrapure water and then dried in an oven at 105°C for 24 hours. The synthesized biochar was termed C.biochar and was utilized for further adsorbing the model dye, i.e., methylene blue (MB dye).

Fe/Mn-C.biochar Composite Synthesis

Wet impregnation techniques [18] with a slight modification were employed to synthesize the Fe/Mn-C. biochar composite. $FeCl_3 \cdot 6H_2O$ and $MnCl_2 \cdot 4H_2O$ served as sources of iron and manganese, respectively. In a typical method, 15 g of Conocarpus pruning waste biomass powder was added to a 180 mL solution of $FeCl_3 \cdot 6H_2O$ (0.70 mol L^{-1}) and $MnCl_2 \cdot 4H_2O$ (0.35 mol L^{-1}). The solution was thoroughly mixed and stirred on a magnetic stirrer plate for 4 hours at 60°C. Subsequently, the slurry was retrieved and dried in a drying oven for 24 hours at 80°C. The dried product was then pyrolyzed under the same conditions as those used to prepare pristine C.biochar. The resulting Fe/Mn-C.biochar composite underwent multiple washes with ultrapure water and was subsequently kept in a drying oven for 24 hours at 105°C. Following the drying process, the composite was stored in a desiccator until further characterization and experiments.

Batch Reactor Adsorption Studies

Batch experiments were performed in the aqueous phase utilizing C.biochar and Fe/Mn-C.biochar composite in the presence of MB dye. The experiments were performed at temperatures of 25±2°C. Erlenmeyer flasks with a capacity of 250 mL were utilized, each having 50 mL of varying initial concentrations of MB dye ranging from 20 to 70 mg L^{-1}. The doses of C.biochar and Fe/Mn-C.biochar composite ranged from 0.10 to 0.4 g L^{-1}. The pH of the solutions was adjusted within the range of 3 to 10 using either 0.1 M HCl or 0.1 M NaOH solutions. The flasks underwent agitation using a shaking incubator operating at 150 rpm for specific contact times ranging from 10 to 180 minutes to achieve equilibrium. Subsequently, the filtrates were examined using a $T80^+$ spectrophotometer (PG instruments) at 668 nm wavelength. The adsorption capacities at time and equilibrium, *i.e.,* q_t and q_e in mg g^{-1}, along with the percentage MB dye removal for both C.biochar and Fe/Mn-C.biochar composite, were determined using Eq. 1–Eq. 3.

$$q_t = \left(\frac{C_o - C_t}{m}\right) \times V \quad (1)$$

$$q_e = \left(\frac{C_o - C_t}{m}\right) \times V \quad (2)$$

$$Removal\,(\%) = \left(\frac{C_o - C_f}{C_o}\right) \times 100 \quad (3)$$

Where: V is volume in L, m is the mass of the adsorbent in g, C_o, C_t, and C_f are the initial, at time "t" and final MB dye concentrations (mg L^{-1}), respectively.

Kinetic Modelling

Kinetic studies on adsorption play a vital role in optimizing the conditions of the adsorption process for the removal of contaminants. In this study, the kinetics of the MB dye adsorption process were examined through commonly used models: the first order (FO) model, the pseudo-second order (PSO) model, and the intraparticle diffusion model (IPD). These models can be mathematically represented by Eq. 4–Eq. 6. The adsorption kinetics were investigated at various initial dye concentrations (20, 30, 40, 50, 60, and 70 mg L^{-1}) over a period of 180 minutes.

$$\ln C_t = -k_t + \ln C_0 \quad (4)$$

$$\frac{t}{q_e} = \frac{1}{k_2 q_e^2} + \frac{1}{q_e} \quad (5)$$

$$q_t = k_{id} t^{0.5} + I \quad (6)$$

Here: k, k_2, and k_{id} denote FO, PSO, and IPD model constants, respectively. I determines the boundary layer thickness in the IPD model.

Adsorption Isotherm Analysis

Adsorption isotherm models are extensively utilized mathematical tools for characterizing various aspects of the adsorption process, such as the extent of molecule coverage, the homogeneity or heterogeneity of the adsorbent surface, the strength of binding energies, the nature of the physical and chemical interactions involved, as well as the adsorption heat of the molecules. In this study, the equilibrium data of MB dye adsorbed on Fe/Mn-C.biochar was analyzed using linearized versions of four commonly employed isotherm models: Langmuir, Freundlich, Temkin, and Dubinin-Radushkevich (D–R). Subsequently, the parameters and constants of these models were calculated based on the obtained results. The linearized forms of the Langmuir, Freundlich, Temkin, and D–R isotherm models are represented by Eq. 7–Eq. 10, respectively.

$$\frac{1}{q_e} = \frac{1}{K_L q_{max}} \times \frac{1}{C_e} + \frac{1}{q_{max}} \quad (7)$$

$$\log q_e = \log K_f + \frac{1}{n} \log C_e \quad (8)$$

$$q_e = B_T \ln A + B_T \ln C_e \quad (9)$$

$$q_e = \ln q_m - K\mathcal{E}^2 \quad (10)$$

Where: q_e and q_{max} are the equilibrium and maximum adsorption capacities, K_L, K_f, B_T and K are the Langmuir, Freundlich, Temkin, and D–R constants, respectively. $\mathcal{E}$ and A are the adsorption potential and equilibrium binding constant, respectively.

Results and Discussion

Characterization

Fourier Transform Infrared Spectroscopy Analysis

The Fourier transform infrared (FTIR) spectra were scanned for the C.biochar, MB dye-loaded C.biochar, Fe/Mn-C.biochar, and Fe/Mn-C.biochar containing MB. The spectrum of all four materials indicated the presence of various functional groups. In all C.biochar and Fe/Mn-C.biochar composites, the peaks at 1024 cm^{-1} are associated with C-O stretching and Fe/Mn-C.biochar displays additional peaks at 444 cm^{-1} (Mn-O), 531 cm^{-1} (Fe-O vibrations) [19], a peak at 1616 cm^{-1} was attributed to aromatic C=C stretching, and peaks at 2845 cm^{-1} and 2910 cm^{-1} were attributed to C-H stretching [20].

In addition, a peak at 3410 cm^{-1} is assigned to the -OH stretching [21]. These results therefore indicate the presence of oxygen-containing groups in aromatic structures and aliphatic hydrocarbons. Nitrogen-containing groups were present at 1016 cm^{-1} (C-N stretching), 1701 cm^{-1}, and 1731 cm^{-1} (C=O stretching) in the MB-loaded nanocomposites [22]. Moreover, vibrations under 600 cm^{-1} represent tensile vibration to metal-based compound formation [23]. As a result of the adsorption process, Mn-O and Fe-O peaks observed in Fe/Mn-C.biochar were reduced, implying interactions of metal oxides with MB dyes to form complexes. These findings were supported by the EDS analysis (Fig. 1b and Fig.1d) that revealed Mn and Fe reduction (weight%) after the adsorption reaction. Previous studies showed that the electrostatic interactions, complexation, or redox reactions with dye molecules are due to the presence of Fe/Mn, which enhances the adsorption capacities of the nanocomposites. The decreased peak intensities were observed and changes in weight% of Mn and Fe indicate that a complexing process occurs between dye molecules trapped by the Fe/Mn oxide presented within C.biochar [24]. The characterization results agree with the reaction studies, as Fe/Mn modified C.biochar showed higher adsorption capacity and percent removal compared to C.biocar.

Scanning Electron Microscopic Analysis

Scanning electron microscopy (SEM) and energy dispersive spectroscopy (EDS) were used to understand the surface morphology of the C.biochar and Fe/Mn-C.biochar before and after the adsorption reaction. Fig. 2a–Fig. 2d illustrates the surface characteristics of C.biochar, Fe/Mn-C.biochar, and MB-loaded C.biochar and Fe/Mn-C.biochar. The images of C.biochar and MB-loaded C.biochar exhibit smooth surfaces, while MB loading is evident in Fig. 2b. Upon the introduction of Fe/Mn- into C.biochar, a distinct spherical shape is observed in Fig. 2c. However, after the adsorption of MB dye, agglomeration becomes apparent. The coexistence of Fe, Mn, and C is evident in the EDS analysis shown in Fig. 2 (1a–1d).

In addition, the EDS analysis depicted that C was the dominant element in both C.biochar and MB-loaded C.biochar (Fig. 2 (1a and 1b)). However, after the wet impregnation process of Fe/Mn introduction, a decrease in C contents (96% to 71%) was observed. The contents (weight%) of Mn and Fe were 2.9 and 9.2, respectively. This implies that more Mn and Fe oxides were impregnated in Fe/Mn-C.biochar, which eventually contributed to the efficient adsorption of MB dye [25]. Moreover, after adsorption of MB dye, the Mn and Fe contents (weight%) decreased to 0.5 and 2.5, respectively (Fig. 2 (1c and 1d)). The reduction in Mn and Fe contents after MB dye adsorption suggests the formation of surface complexes or coordination bonds, likely involving hydrogen bonding, π–π interactions, and ion exchange processes between the metal oxides and dye molecules on the biochar surface [26].

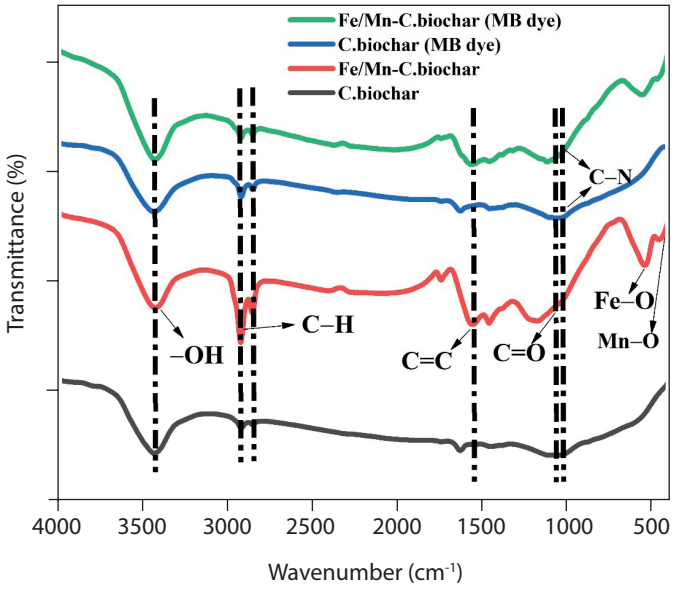

Fig. 1. FTIR analysis of the C.biochar, MB loaded C.biochar, Fe/Mn-C.biochar, and MB loaded Fe/Mn-C.biochar.

a)

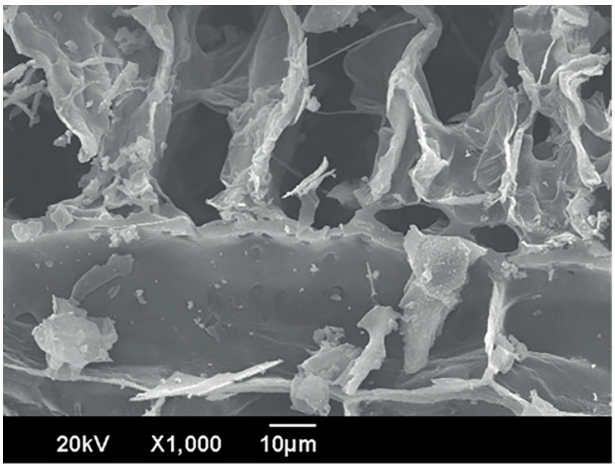

b)

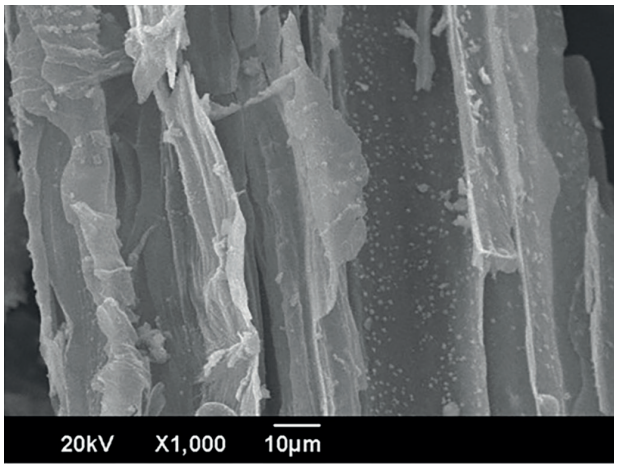

1a)

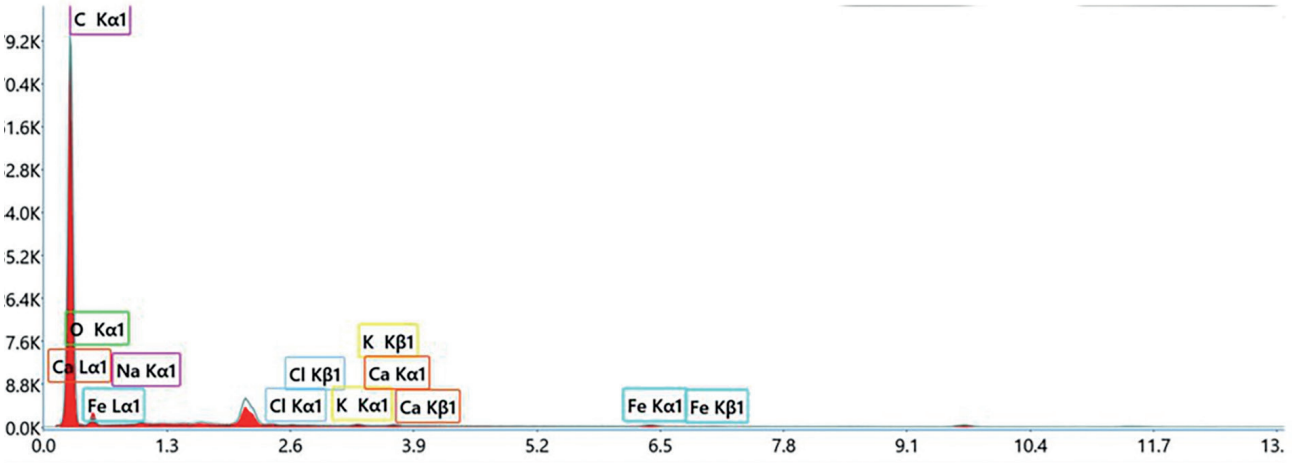

1b)

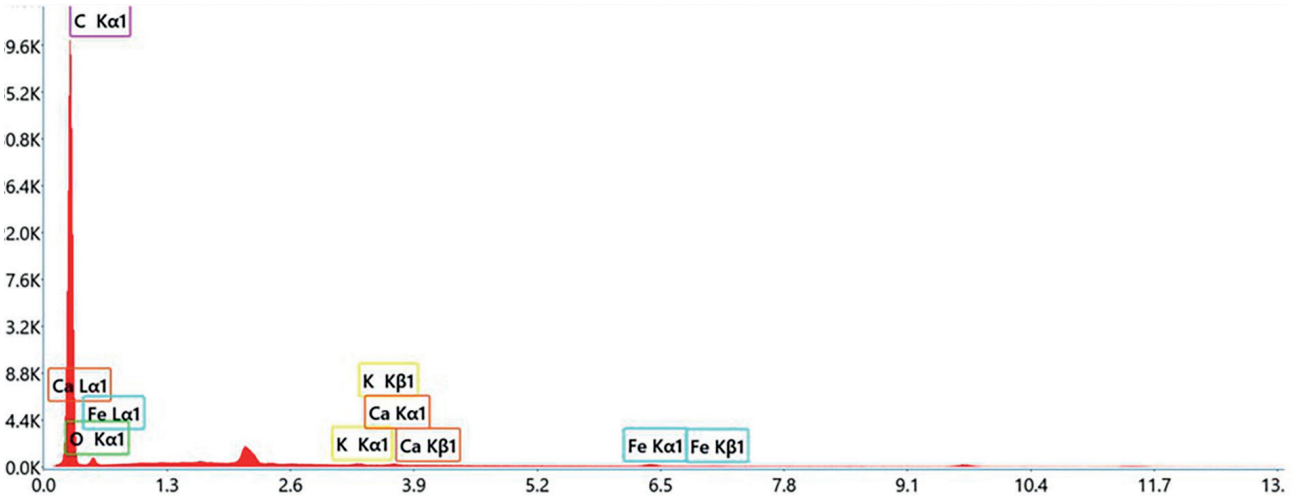

Fig. 2. Surface morphology studies. a) C.biochar; b) MB loaded C.biochar; 1a) C.biochar; 1b) MB loaded C.biochar; 1c) Fe/Mn-C. biochar; 1d) MB loaded Fe/Mn-C.biochar.

c)

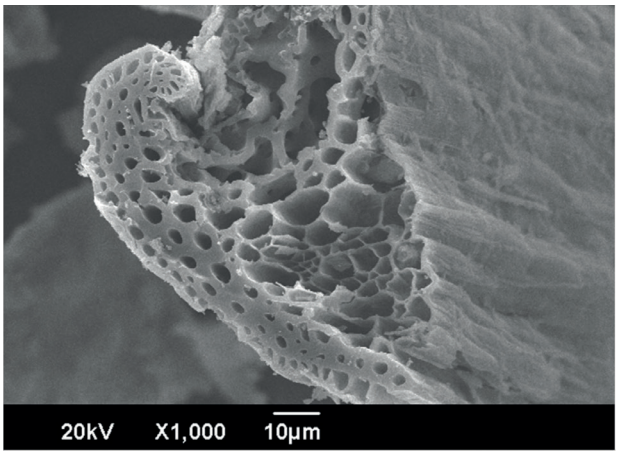

d)

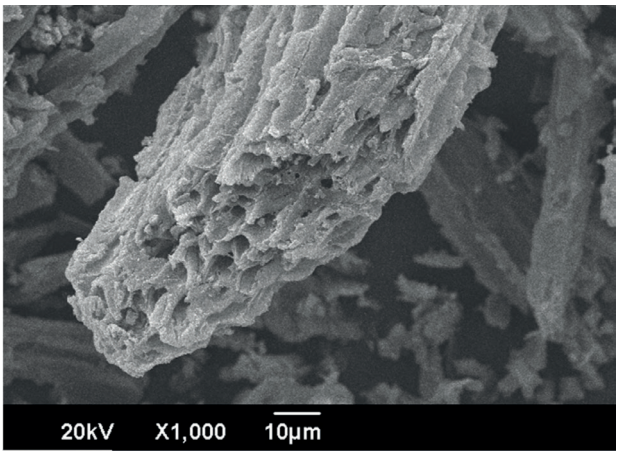

1c)

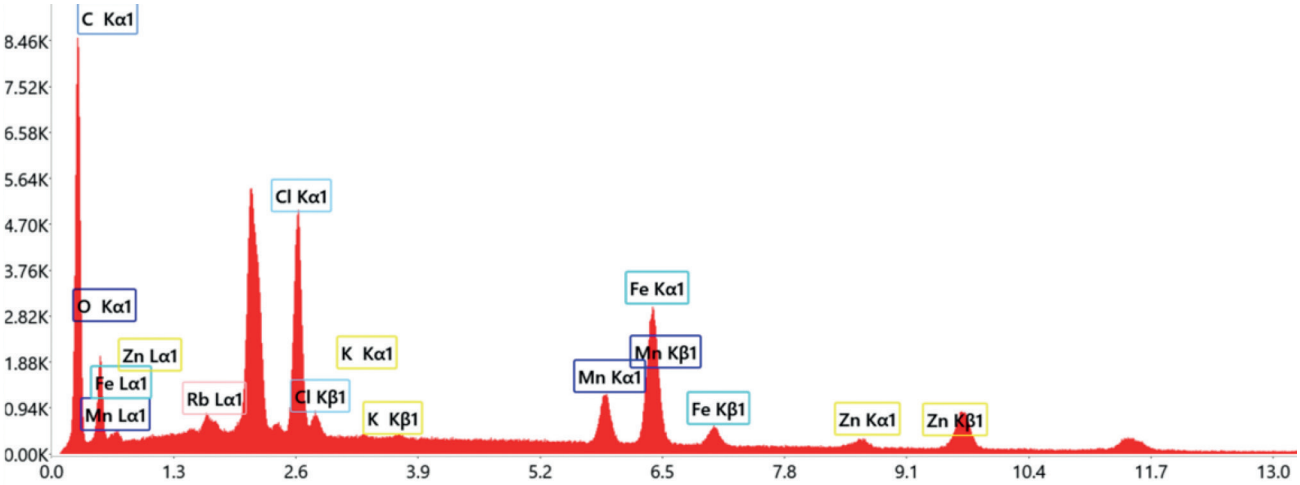

1d)

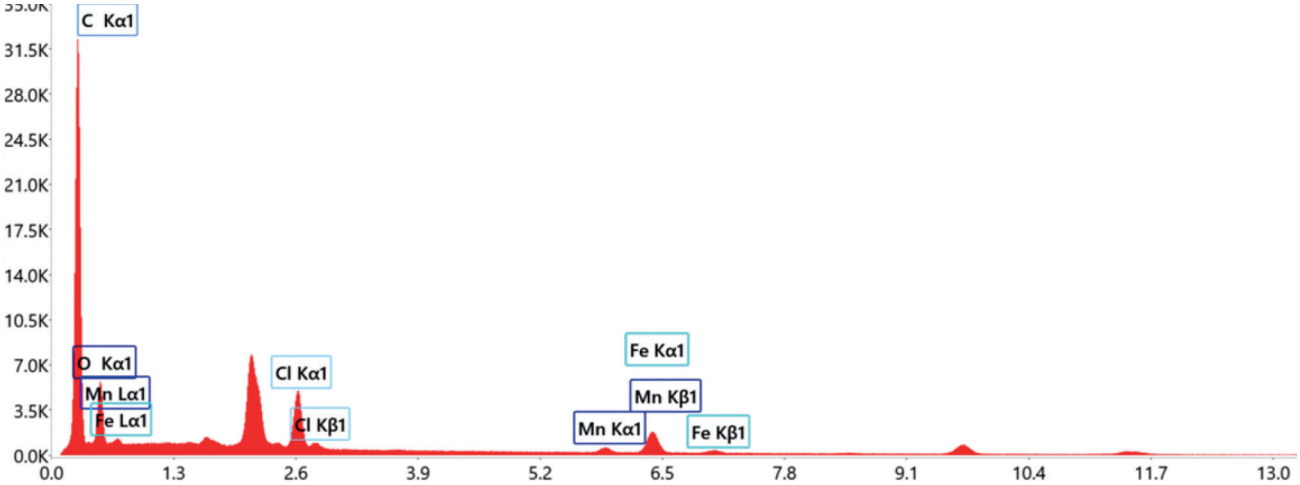

Fig. 2 cont. Surface morphology studies. c) Fe/Mn-C.biochar; d) MB loaded Fe/Mn-C.biochar. EDX analysis.

Effect of Different Reaction Parameters

Effect of Contact Time

MB dye adsorption was studied across a wide range of contact times, ranging from 0 to 180 minutes. The data collected demonstrates a gradual increase in the adsorption capacity of MB dye over time, as clearly illustrated in Fig. 3. The maximum adsorption capacity of 97.41 mg g^{-1} (97.38%) was achieved at 60 minutes, with no further notable increase in the adsorption. This phenomenon can be attributed to the abundance of unoccupied sites initially present on the surface of the Fe/Mn-C.biochar composite [27], which facilitates the rapid adsorption of MB. Moreover, as time progresses, the remaining unoccupied sites become less accessible to the MB dye molecules due to potential repulsion between the already adsorbed molecules and the molecules present in the solution [28]. The point of equilibrium signifies the instance when the absorbent reaches a state of saturation and can no longer adsorb additional dye molecules. Consequently, no further enhancement in the MB adsorption capacity was observed after 60 minutes. This moment was designated as the equilibrium time, prompting the execution of the rest of the batch experiments to explore the remaining influential factors until equilibrium was attained.

Effect of Adsorbent Dose

The effect of the amount of C.biochar and Fe/Mn-C. biochar composite on the adsorption of MB dye was observed by adsorbing a constant concentration of dye (40 mg L^{-1}) at varying amounts (0.1 to 0.4 g L^{-1}) under ambient conditions as depicted in Fig. 4a and Fig. 4b. The increase in adsorbent dosage resulted in an increase in MB removal for both C.biochar and its nanocomposites. This phenomenon can be ascribed to an increased quantity of available sites for adsorption. When the dose of C.biochar and Fe/Mn-C.biochar composite was 0.1 g L^{-1}, the adsorption capacity for MB was 38.51 mg g^{-1} (9.624% removal) and 159.55 mg g^{-1} (39.87% removal), respectively. Upon increasing the adsorbent dose to 0.4 g L^{-1}, the removal percentage for C.biochar and Fe/Mn-C.biochar composite increased to 18.32% and 97.38% respectively. However, the adsorption capacity decreased to 18.33 mg g^{-1} for C.biochar and 97.41 mg g^{-1} for Fe/Mn-C.biochar composite. The elevated concentration of MB in the system for lower amounts of the adsorbent indicates the presence of numerous active sites for adsorption and consequently a high adsorption capacity. However, as the amount of adsorbent continues to increase, the removal rate tends to increase because more empty adsorption sites become available. However, once the MB adsorption amount reaches saturation, the removal rate does not increase even if the amount of adsorbent is increased. The observed trend of higher adsorption capacity at low adsorbent doses with lower MB removal percentages, and vice versa at higher doses, can be attributed to various factors in the adsorption processes. Initially, at a low dosage of the composite, the underutilization of available surface sites and faster mass transfer contribute to an increased adsorption capacity [29] but decreased removal percentages. As the adsorbent dose increases, surface saturation, aggregation of adsorbent particles, mass transfer limitations, competition for active sites, and diffusion constraints within particles become prominent [30], leading to a decrease in adsorption capacity but higher removal percentages.

Effect of pH

Solution pH is also a crucial determinant in the adsorption of MB onto the absorbents. Fig. 5a and b depicted the MB removal efficacy and adsorption capacity of C.biochar and Fe/Mn-C.biochar nanocomposite at a series of pH values (3–10). The adsorption of MB on both absorbents consistently increased as the pH increased. For C.biochar, the removal percentage was recorded between 15 to 19% at a pH range of 3 to 10. However, the introduction of Fe and Mn led to a sharp increase in the removal percentage for both acidic and alkaline pH ranges. With

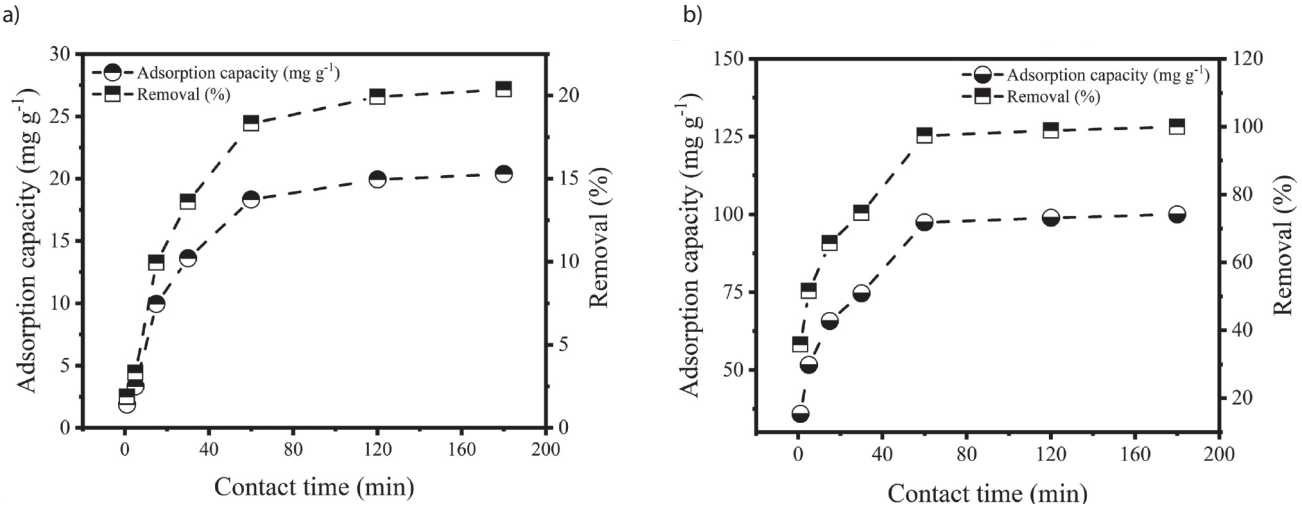

Fig. 3. Effect of contact time on the MB adsorption. a) C.biochar; b) Fe/Mn-C.biochar composite.

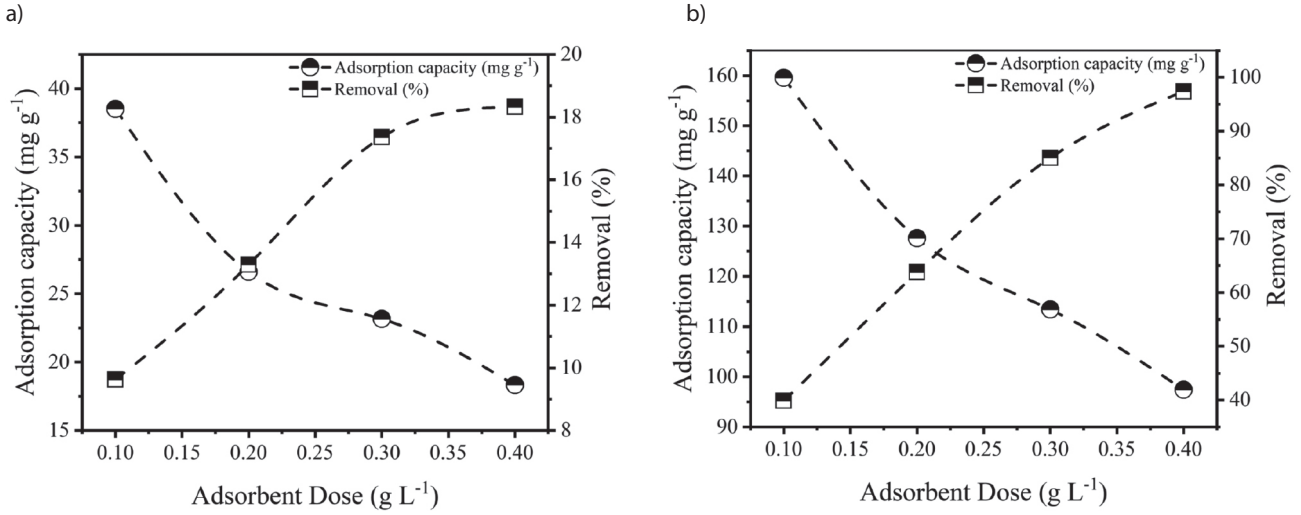

Fig. 4. Effect of adsorbent dose on the MB adsorption. a) C.biochar; b) Fe/Mn-C.biochar composite.

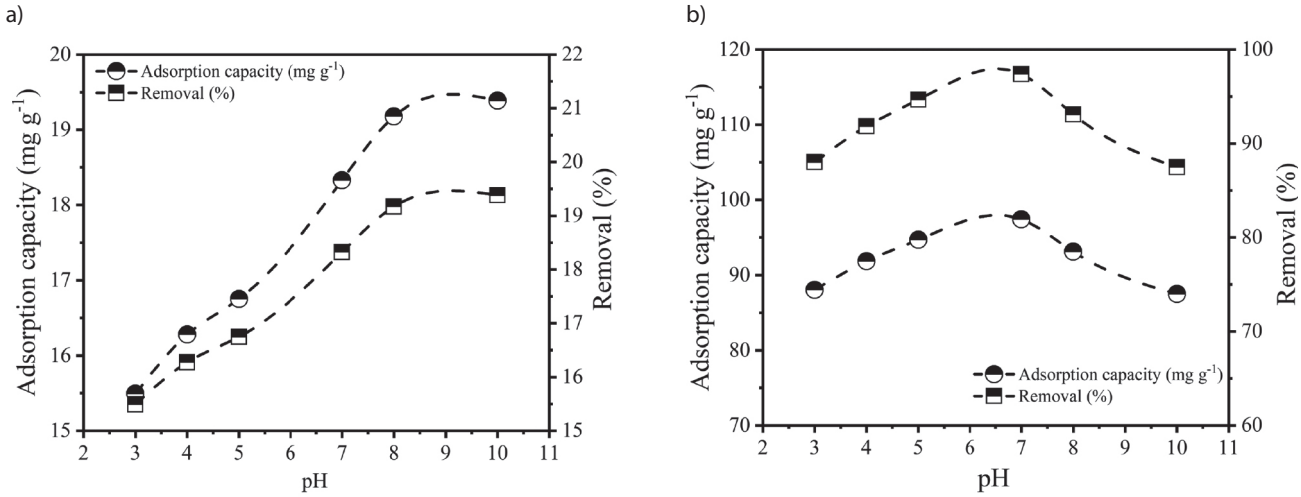

Fig. 5. Effect of pH on the adsorption of MB. a) C.biochar; b) Fe/Mn-C.biochar composite.

an increase in pH (3−10), the MB removal rate reached approximately 90%, and at pH >7, the removal rate was almost 100% for Fe/Mn-C.biochar. This information illustrates the importance of an electrostatic interaction binding mechanism. The biochar surface exhibits chemical groups such as -OH and -COOH, and the dye pH induces alterations in the charge and electrical properties of these groups [31]. When pH is lower, the absorbent surface is enriched with a notable amount of H^+ ions, leading to electrostatic repulsion with the cationic dye (MB) [32], thereby impeding MB adsorption. With the rise in pH, the H^+ ions concentration reduced, attenuating the specific reaction and competitive adsorption between MB and H^+, ultimately resulting in improved MB dye adsorption.

Effect of MB Concentration

Investigations of the removal efficiency of C.biochar and Fe/Mn-C.biochar nanocomposite for different initial MB concentrations ranging from 20 to 70 mg L^{-1} were conducted. Fig. 6a illustrates the initial adsorption and removal rate of MB solution over C.biochar. In the beginning, the removal rate reached 27%. However, as the initial concentration increased, the removal rate gradually decreased. In the case of Fe/Mn-C.biochar, the removal rate was nearly 100% at 20 mg L^{-1} MB concentration but decreased to 66.51% when the concentration reached 70 mg L^{-1} (Fig 6b). The observed decrease in the percent removal could be attributed to the reduced availability of active sites necessary for higher dye concentrations. Conversely, the adsorption capacity exhibited a rapid increase with higher solution concentrations, primarily due to the intensified adsorption driving force and enhanced contact between the adsorbent and MB dye. At 70 mg L^{-1} MB concentration, the adsorption capacity reached an impressive 116.41 mg g^{-1}. As MB concentration increases, more dye molecules are available for adsorption, leading to an apparent increase in adsorption capacity [33]. However, the higher concentration may also result in increased competition among dye molecules for available adsorption sites, possibly leading to incomplete

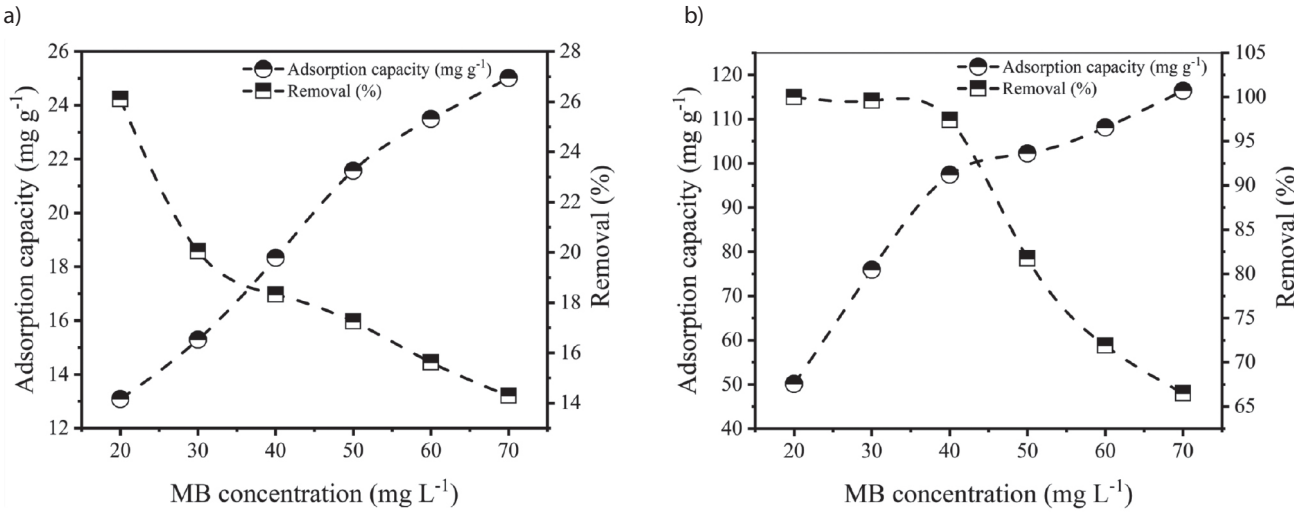

Fig. 6. Effect of MB concentration on the % removal and adsorption capacity. a) C.biochar; b) Fe/Mn-C.biochar composite.

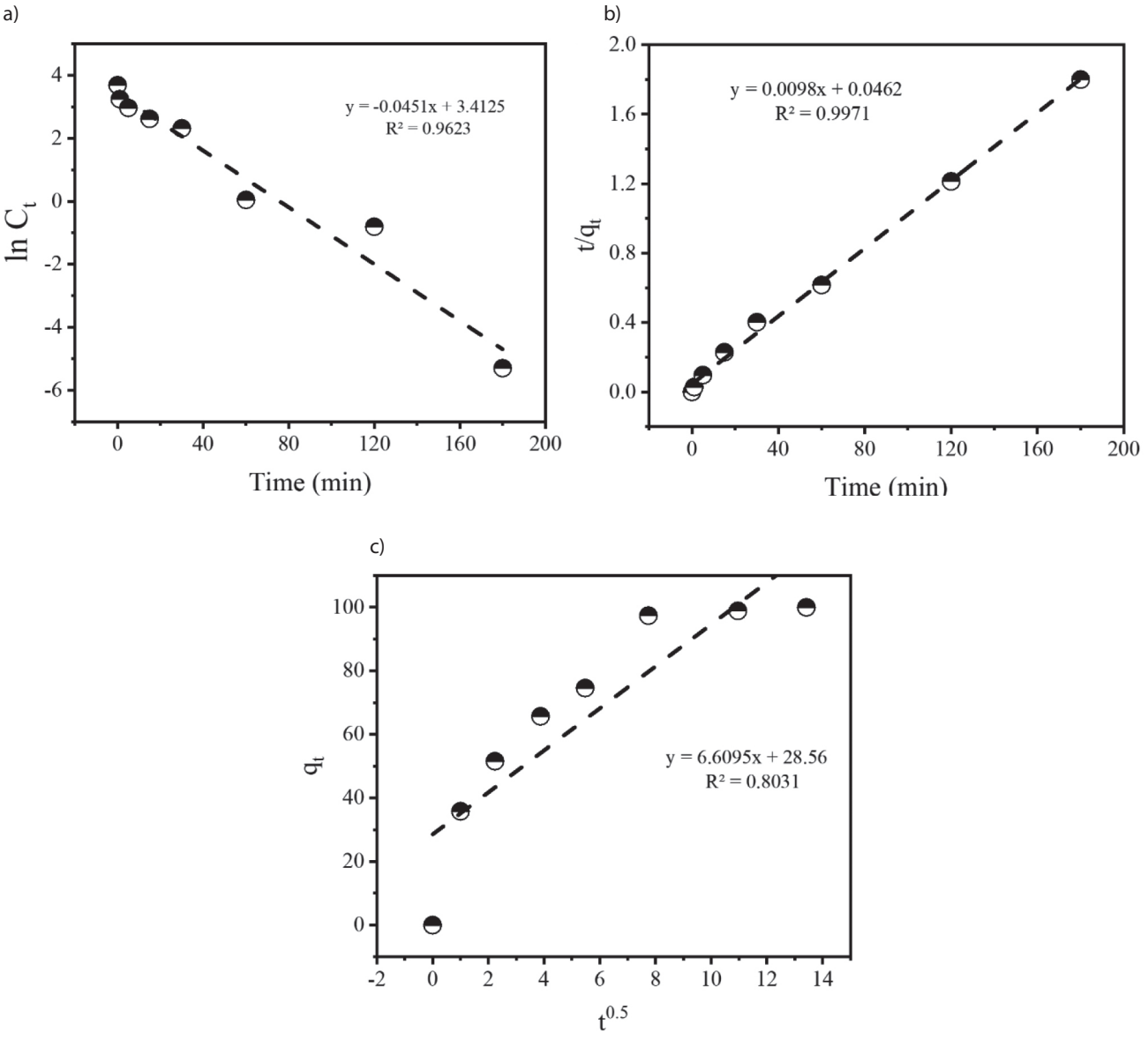

Fig. 7. Adsorption kinetics. a) first order; b) pseudo second order; c) Intra particle diffusion model.

Table 1. Kinetic parameters and constant for first order, pseudo second order, and Intra particle diffusion model fitness.

FO		PSO		IPD	
C_0	30.341	q_e (cal)	102.04	k_{id}	6.60
$t^{0.5}$	15.36	q_e (exp)	97.38	I (thickness)	28.56
k	0.0451	k_2	0.002	R^2	0.8031
R^2	0.9623	R^2	0.9971		

coverage of the adsorbent surface and reduced removal efficiency [34]. Furthermore, when the concentration of dye is increased to a point of saturation, this could lead to a reduction in the overall removal rate but higher adsorption capacity as the active sites may become saturated more quickly [35]. These results reveal the importance of the concentration effects and support the use of Fe/Mn-C. biochar nanocomposites in wastewater treatment processes.

Adsorption Kinetics

The adsorption mechanism of the Fe/Mn-C.biochar nanocomposite was studied by fitting the data in FO, PSO, and IPD kinetic models. Table 1 depicts the kinetic parameters. Fig. 7a shows that a straight line ($R^2 = 0.9623$) in the FO kinetic fitting was obtained by the linear fit, however, differences were observed in the calculated and experimental initial concentrations (30.34 mg L^{-1} and 40 mg L^{-1} respectively). On the contrary, the linear fitting performance of the pseudo-second-order dynamic model was outstanding, showing minimal deviation between the experimental (97.38 mg g^{-1}) and calculated qe (102.04 mg g^{-1}) (Fig. 7b). The correlation coefficient (R^2) for fitting the adsorption process of the Fe/Mn-C. biochar composite under various initial MB concentrations using the pseudo-second-order kinetic equation was 0.9971 (Table 1). This result suggests that the pseudo-second-order model provides a more accurate description

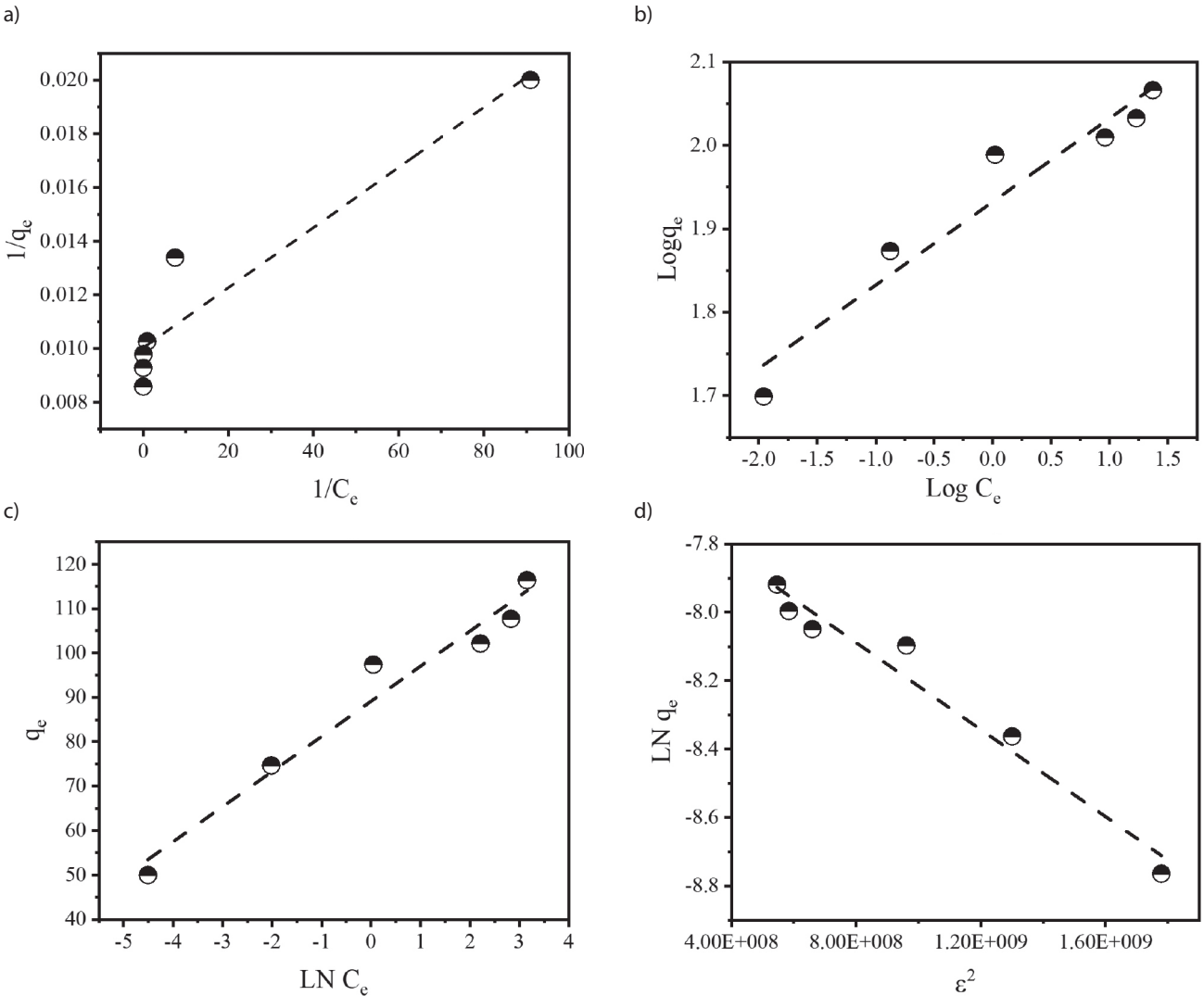

Fig. 8. Adsorption isotherm analysis. a) Langmuir; b) Freundlich; c) Temkin; d) D–R isotherm model.

of MB adsorption onto the Fe/Mn-C.biochar composite. It implies the potential engagement of multiple adsorption mechanisms [36]. Earlier studies have shown that the rate of MB adsorption onto porous carbonaceous materials is predominantly governed by internal diffusion within the particles [36]. To confirm this phenomenon, an intra-particle diffusion model was employed. The linear plot of q versus $t^{0.5}$, yielding I (mg g^{-1}) and K_{id} (mg g^{-1} $min^{-1/2}$) from the intercept and slope, respectively, indicates that the IPD model explains the adsorption phenomenon well, with a coefficient of determination (> 0.80) (Fig. 7c)). The high K_{id} values further signify the involvement of diffusion processes in MB dye uptake by the Fe/Mn-C.biochar.

Adsorption Isotherm Studies

In Fig. 8, the adsorption isotherms for MB on Fe/ /Mn-C.biochar using Langmuir, Freundlich, Temkin, and Dubinin-Radushkevich (D–R) isotherm models are depicted, while Table 2 presents different kinetic parameters of these models. The Langmuir isotherm (Fig.8a), assuming monolayer adsorption on a homogeneous surface with uniform energy sites, exhibited a good fit (R^2 = 0.9018) to the experimental data, with R_L values ranging from 0 to 1, signifying favorable adsorption [37]. The experimentally determined adsorption capacity (97.38 mg g^{-1}) closely matched the modeled maximum capacity (99.70 mg g^{-1}), reinforcing Fe/Mn-C.biochar composite suitability for MB adsorption.

The Freundlich isotherm (Fig. 8b), reflecting multilayer adsorption on a heterogeneous surface, demonstrated favorable MB adsorption on Fe/Mn-C.biochar, supported by an increase in adsorption capacity (K_f) [38]. The experimental data showed a good fit to the Freundlich model (R^2 = 0.93), indicating its appropriateness for describing the adsorption process. The Temkin isotherm (Fig. 8c), which considers a linear decline in adsorption heat [39], exhibited a superior fit (R^2 = 0.96) compared to Langmuir, Freundlich, and D–R models. Lastly, the D–R isotherm (Fig. 8d), assessing the potential energy distribution of adsorption sites [40], displayed a good fit (R^2 = 0.96) but yielded a mean free energy value (E) of 2.8×10^4 kJ·mol^{-1}, indicative of chemisorption. This comprehensive analysis of various isotherm models enhances our understanding of the intricate adsorption behavior of MB on Fe/Mn-C. biochar.

Table 2. Langmuir, Freundlich, Temkin, and D–R isotherm parameters.

Model	Parameters	Value
Langmuir	q_e (mg g^{-1})	97.38
	q_{max} (mg g^{-1})	99.70
	K_L (L mg^{-1})	89.47
	R^2	0.9018
Freundlich	1/n	0.0999
	K_f (L g^{-1})	85.54
	R^2	0.9355
Temkin	BT	7.9053
	A	78743.85
	bt	310.4091
	R^2	0.9617
D–R	q_{DR} (mol g^{-1})	0.00051
	β (mol $J^{-1})^2$	3.09×10^3
	E (kJ mol^{-1})	2.89×10^4
	R^2	0.9606

Conclusions

Fe/Mn-C.biochar composite was synthesized from Conocarpus (pruning wood waste) biochar using a modified wet impregnation method. Different characterization techniques were employed to study the physicochemical properties of the synthesized nanocomposites. FTIR analysis indicated the presence of various functional groups, including C-O stretching, aromatic C=C stretching, and C-H stretching. Fe/Mn-Biochar exhibited additional peaks associated with metal-oxygen vibrations below 600 cm^{-1}. Subsequent investigations on MB adsorption revealed that Fe/Mn-Biochar demonstrated higher removal efficiency (100%) compared to biochar (25%). The adsorption capacity increased with contact time until equilibrium was reached at 60 minutes. pH influenced adsorption, with Fe/Mn-Biochar showing enhanced removal at both acidic and alkaline pH values. The adsorption capacity increased with the initial MB concentration, but higher concentrations led to increased competition among dye molecules for available sites, impacting removal efficiency. Adsorption kinetics revealed that the pseudo-second-order model best described the MB adsorption onto Fe/Mn-C.biochar. Adsorption isotherm studies using Langmuir, Freundlich, Temkin, and Dubinin-Radushkevich models highlighted the suitability of Fe/Mn-C.biochar for MB adsorption, with the Temkin and D–R model providing the best fit and indicating chemisorption. Overall, the findings suggest that the introduction of Fe/Mn in biochar enhances its adsorption capabilities, potentially through a combination of surface complexation and metal ion interactions.

Acknowledgments

The project was financially supported by the Vice Deanship of Research Chairs, King Saud University, Riyadh, KSA.

Conflict of Interest

The authors declare no conflict of interest.

References

1. DENICOLA E., ABURIZAIZA O.S., SIDDIQUE A., KHWAJA H., CARPENTER D.O. Climate Change and Water Scarcity: The Case of Saudi Arabia. Annals of Global Health, **81** (3), 342, **2015**.
2. SHAFIQ M., ALAZBA A.A., AMIN M.T. Preparation of ZnMgAl-Layered double hydroxide and rice husk biochar composites for Cu(II) and Pb(II) ions removal from synthetic wastewater. Water, **15** (12), 2207, **2023**.
3. EMILE R., CLAMMER J.R., JAYASWAL P., SHARMA P. Addressing water scarcity in developing country contexts: a socio-cultural approach. Humanities and Social Sciences Communications, **9** (1), 1, **2022**.
4. AMIN M.T., ALAZBA A.A., SHAFIQ M. NiFe-Layered double hydroxide nanocomposites with functionalized bentonite clay to attenuate lead ions in wastewater: isothermal and kinetic studies. Water, Air, & Soil Pollution, **234** (7), 430, **2023**.
5. KHAN I., SAEED K., ZEKKER I., ZHANG B., HENDI A.H., AHMAD A., AHMAD S., ZADA N., AHMAD H., SHAH L.A., SHAH T., KHAN I. Review on methylene blue: its properties, uses, toxicity and photodegradation. Water, **14** (2), 242, **2022**.
6. BENNETT N.J., ALAVA J.J., FERGUSON C.E., BLYTHE J., MORGERA E., BOYD D., CÔTÉ I. M. Environmental (in)justice in the Anthropocene ocean. Marine Policy, **147**, 105383, **2023**.
7. AZIMI B., SEPAHVAND S., ISMAEILIMOGHADAM S., KARGARZADEH H., ASHORI A., JONOOBI M., DANTI S. Application of cellulose-based materials as water purification filters; A state-of-the-art review. Journal of Polymers and the Environment, **32** (1), 345, **2024**.
8. QIU B., SHAO Q., SHI J., YANG C., CHU H. Application of biochar for the adsorption of organic pollutants from wastewater: Modification strategies, mechanisms and challenges. Separation and Purification Technology, **300**, 121925, **2022**.
9. ALI H., AHMED S., HSINI A., KIZITO S., NACIRI Y., DJELLABI R., ABID M., RAZA W., HASSAN N., SAIF UR REHMAN M., JAMAL KHAN A., KHAN M., ZIA UL HAQ M., ABOAGYE D., KASHIF IRSHAD M., HASSAN M., HAYAT A., WU BO., QADEER A., AJMAL Z. Efficiency of a novel nitrogen-doped Fe_3O_4 impregnated biochar (N/Fe_3O_4@BC) for arsenic (III and V) removal from aqueous solution: Insight into mechanistic understanding and reusability potential. Arabian Journal of Chemistry, **15** (11), 104209, **2022**.
10. CHEN W.-H., HOANG A.T., NIŽETIĆ S., PANDEY A., CHENG C.K., LUQUE R., ONG H.C., THOMAS S., NGUYEN X.P. Biomass-derived biochar: From production to application in removing heavy metal-contaminated water. Process Safety and Environmental Protection, **160**, 704, **2022**.
11. LUO Z., YAO B., YANG X., WANG L., XU Z., YAN X., TIAN L., ZHOU H., ZHOU Y. Novel insights into the adsorption of organic contaminants by biochar: A review. Chemosphere, **287**, 132113, **2022**.
12. JHA S., GAUR R., SHAHABUDDIN S., TYAGI I. Biochar as sustainable alternative and green adsorbent for the remediation of noxious pollutants: A Comprehensive Review. Toxics, **11** (2), 117, **2023**.
13. SHI Q., DENG S., ZHENG Y., DU Y., LI L., YANG S., ZHANG G., DU L., WANG G., CHENG M., LIU Y. The application of transition metal-modified biochar in sulfate radical based advanced oxidation processes. Environmental Research, **212**, 113340, **2022**.
14. WEIDNER E., KARBASSIYAZDI E., ALTAEE A., JESIONOWSKI T., CIESIELCZYK F. Hybrid metal oxide/biochar materials for wastewater treatment technology: A review. ACS Omega, **7** (31), 27062, **2022**.
15. LIU W., LI X., CHU X., ZUO S., GAO B., YAO C., LI Z., CHEN Y. Boosting photocatalytic reduction of nitrate to ammonia enabled by perovskite/biochar nanocomposites with oxygen defects and O-containing functional groups. Chemosphere, **294**, 133763, **2022**.
16. XU L., HE Z., WEI X., SHANG Y., SHI J., JIN X., BAI X., SHI X., JIN P. Facile-prepared Fe/Mn co-doped biochar is an efficient catalyst for mediating the degradation of aqueous ibuprofen via catalytic ozonation. Chemical Engineering Journal, **461**, 142028, **2023**.
17. PARTHASARATHY P., SAJJAD S., SALEEM J., ALHERBAWI M., MCKAY G. A review of the removal of dyestuffs from effluents onto biochar. Separations, **9** (6), 139, **2022**.
18. LI L., LAI C., HUANG F., CHENG M., ZENG G., HUANG D., LI B., LIU S., ZHANG M., QIN L., LI M., HE J., ZHANG Y., CHEN L. Degradation of naphthalene with magnetic bio-char activate hydrogen peroxide: Synergism of bio-char and Fe–Mn binary oxides. Water Research, **160**, 238, **2019**.
19. ZENG H., QI W., ZHAI L., WANG F., ZHANG J., LI D. Magnetic biochar synthesized with waterworks sludge and sewage sludge and its potential for methylene blue removal. Journal of Environmental Chemical Engineering, **9** (5), 105951, **2021**.
20. LIU X.-J., LI M.-F., SINGH S.K. Manganese-modified lignin biochar as adsorbent for removal of methylene blue. Journal of Materials Research and Technology, **12**, 1434, **2021**.
21. SINGH S.K., DHEPE P.L. Isolation of lignin by organosolv process from different varieties of rice husk: Understanding their physical and chemical properties. Bioresource Technology, **221**, 310, **2016**.
22. ZHANG P., O'CONNOR D., WANG Y., JIANG L., XIA T., WANG L., TSANG D.C.W., OK Y.S., HOU D. A green biochar/iron oxide composite for methylene blue removal. Journal of Hazardous Materials, **384**, 121286, **2020**.
23. GUADIX-MONTERO S., SANKAR M. Review on catalytic cleavage of C–C inter-unit linkages in lignin model compounds: Towards Lignin Depolymerisation. Topics in Catalysis, **61** (3), 183, **2018**.
24. TANG S.-F., ZHOU H., TAN W.-T., HUANG J.-G., ZENG P., GU J.-F., LIAO B.-H. Adsorption characteristics and mechanisms of Fe-Mn oxide modified biochar for Pb(II) in wastewater. International Journal of Environmental Research and Public Health, **19** (14), 8420, **2022**.
25. WANG S., GAO B., LI Y., WAN Y., CREAMER A.E. Sorption of arsenate onto magnetic iron-manganese (Fe–Mn) biochar composites. RSC Advances, **5** (83), 67971, **2015**.
26. YIN G., SONG X., TAO L., SARKAR B., SARMAH A.K., ZHANG W., LIN Q., XIAO R., LIU Q., WANG H. Novel Fe-Mn binary oxide-biochar as an adsorbent for removing Cd(II) from aqueous solutions. Chemical Engineering Journal, **389**, 124465, **2020**.
27. REHMAN S., ADIL A., SHAIKH A.J., SHAH J.A., ARSHAD M., ALI M.A., BILAL M. Role of sorption energy and chemisorption in batch methylene blue and Cu^{2+} adsorption by novel thuja cone carbon in binary component system: linear and nonlinear modeling. Environmental Science and Pollution Research, **25** (31), 31579, **2018**.

28. SARWAR A., WANG J., KHAN M.S., FAROOQ U., RIAZ N., NAZIR A., MAHMOOD Q., HASHEM A., AL-ARJANI A.-B.F., ALQARAWI A.A., ABD_ALLAH E.F. Iron oxide (Fe_3O_4)-supported SiO_2 magnetic nanocomposites for efficient adsorption of fluoride from drinking water: synthesis, characterization, and adsorption isotherm analysis. Water, **13** (11), 1514, **2021**.
29. HASSAN M.M., CARR C.M. Biomass-derived porous carbonaceous materials and their composites as adsorbents for cationic and anionic dyes: A review. Chemosphere, **265**, 129087, **2021**.
30. SINGH K.P., MOHAN D., SINHA S., TONDON G.S., GOSH D. Color removal from wastewater using low-cost activated carbon derived from agricultural waste material. Industrial & Engineering Chemistry Research, **42** (9), 1965, **2003**.
31. GUO D., LI Y., CUI B., HU M., LUO S., JI B., LIU Y. Natural adsorption of methylene blue by waste fallen leaves of Magnoliaceae and its repeated thermal regeneration for reuse. Journal of Cleaner Production, **267**, 121903, **2020**.
32. FAN S., WANG Y., WANG Z., TANG J., TANG J., LI X. Removal of methylene blue from aqueous solution by sewage sludge-derived biochar: Adsorption kinetics, equilibrium, thermodynamics and mechanism. Journal of Environmental Chemical Engineering, **5** (1), 601, **2017**.
33. SINGH S., PRAJAPATI A.K., CHAKRABORTY J.P., MONDAL M.K. Adsorption potential of biochar obtained from pyrolysis of raw and torrefied Acacia nilotica towards removal of methylene blue dye from synthetic wastewater. Biomass Conversion and Biorefinery, **13** (7), 6083, **2023**.
34. LI Y., ZIMMERMAN A.R., HE F., CHEN J., HAN L., CHEN H., HU X., GAO B. Solvent-free synthesis of magnetic biochar and activated carbon through ball-mill extrusion with Fe_3O_4 nanoparticles for enhancing adsorption of methylene blue. Science of The Total Environment, **722**, 137972, **2020**.
35. KHAN M.S., RIAZ N., REHMAN S., CHENHUI L., SHAIKH A.J., ARFAN M., ZEB I., ARSHAD M., HAFEEZ F., BILAL M. Improved photocatalytic decolorization of reactive black 5 dye through synthesis of graphene quantum dots–nitrogen-doped TiO_2. Environmental Science and Pollution Research, **30** (60), 124992, **2023**.
36. YAO Y., BING H., FEIFEI X., XIAOFENG C. Equilibrium and kinetic studies of methyl orange adsorption on multiwalled carbon nanotubes. Chemical Engineering Journal, **170** (1), 82, **2011**.
37. SHAH J.A., BUTT T.A., MIRZA C.R., SHAIKH A.J., KHAN M.S., ARSHAD M., RIAZ N., HAROON H., GARDAZI S.M.H., YAQOOB K., BILAL M. Phosphoric acid activated carbon from *Melia azedarach* waste sawdust for adsorptive removal of reactive orange 16: Equilibrium modelling and thermodynamic analysis. Molecules, **25** (9), 2118, **2020**.
38. YAO X., JI L., GUO J., GE S., LU W., CAI L., WANG Y., SONG W., ZHANG H. Magnetic activated biochar nanocomposites derived from wakame and its application in methylene blue adsorption. Bioresource Technology, **302**, 122842, **2020**.
39. HAROON H., SHAH J.A., KHAN M.S., ALAM T., KHAN R., ASAD S.A., ALI M.A., FAROOQ G., IQBAL M., BILAL M. Activated carbon from a specific plant precursor biomass for hazardous Cr(VI) adsorption and recovery studies in batch and column reactors: Isotherm and kinetic modeling. Journal of Water Process Engineering, **38**, 101577, **2020**.
40. MAJD M.M., KORDZADEH-KERMANI V., GHA-LANDARI V., ASKARI A., SILLANPÄÄ M. Adsorption isotherm models: A comprehensive and systematic review (2010−2020). Science of The Total Environment, **812**, 151334, **2022**.